Benefits of X-Ray CMT for the Modeling of C/C Composites

Olivia Coindreau, Christianne Mulat, Christian Germain, Jean Lachaud, Gerard L. Vignoles

DOI: 10.1002/adem.201000233

Benefits of X-ray CMT for the modelling of C/C composites **

By *O. Coindreau, C. Mulat, C. Germain*, *J. Lachaud*, and *G. L. Vignoles**

[*] *Prof. Dr. G. L. Vignoles, Dr. O. Coindreau, Dr. C. Mulat, Dr. J. Lachaud*
LCTS – UMR 5801 CNRS-Université Bordeaux 1-Safran-CEA,
3, Allée La Boëtie, Pessac, F33600, France
E-mail: vinhola@lcts.u-bordeaux1.fr
Prof. Dr. C. Germain, Dr. C. Mulat
IMS - UMR5218 CNRS-Université Bordeaux 1-IPB
351, Avenue de la Libération, Talence, F33410, France

[**] *This work has been funded by CNRS and Snecma Propulsion Solide (Safran Group) through a grant to O.C., by the French Ministry of Education through a grant to C. M. and by CEA and CNRS through a grant to J. L .*

C/C composites have application in very demanding areas like aerospace, fusion technology, etc ... and thus their optimization is crucial, both in the control of processing routes and in the prediction of their behaviour in use. Intense modelling efforts have been performed in these directions.

To help a direct application on actual materials, with possibly complex reinforcement architectures, X-ray Computerized Micro-Tomography (CMT) is a beneficial technique, since it allows producing extremely detailed representations of these architectures. However, there is a long way from the crude X-ray projections to the information that is directly usable in C/C composite modelling. This article summarizes several achievements in this domain and discusses the obtained results, concerning (i) composites imaging by phase contrast CMT and holographic CMT, (ii) evaluation of effective geometrical and transfer properties in fibre arrangements and actual fibre-reinforced composites, (iii) modelling of degradation by ablation and (iv) modelling of processing by chemical vapour infiltration.

Fibre-reinforced carbon-matrix (C/C) composites are dedicated to very high-performance and high-cost applications, mainly in the domain of aerospace technology,[1] as thermal protection systems, rocket engine hot parts, or aircraft brakes, as well as plasma-facing components in

Tokamak reactors.[2] Design, fabrication and characterization of this class of materials involve large efforts towards the best possible quality, in terms of mechanical and thermal performances, and resistance to physico-chemical erosion. Since the fabrication processes and the high-temperature tests are extremely expensive, there is an evident interest in increasing as much as possible the knowledge on the involved physics and chemistry, in order to produce reliable modelling approaches. One part of the knowledge on the C/C materials that has to enter the modelling approaches is a sound description of the composite morphology, which may be rather complex in some cases. This is where the use of X-ray Computed Micro-Tomography brings help, because of its exceptional capacity for the acquisition of large, accurate 3D images of the material structure.

There are various stages of the material life where X-ray CMT has an interest: first, in the study of the material fabrication, when the carbon matrix is progressively inserted in the arrangement of carbon fibres; second, when the composite is ready for use and one wants to evaluate its properties; third, when it is used in a harsh environment, in order to evaluate its degradation. In this paper, we will try to review some CMT-based modelling efforts in these three directions. The first part will address the preliminary duty of 3D image (block) acquisition, which in the case of synchrotron X-ray CMT is already an issue; the second part recalls some results on the assessment of geometrical and transport properties in C fibre preforms partly infiltrated with C matrix, and addresses infiltration modelling; and the third one discusses the use of CMT for the characterization, modelling and simulation of C/C composite ablation. Finally, some conclusive remarks and guidelines are given.

Image acquisition and processing

In order to have a good representation of the C/C composite architecture, CMT scans may be performed at various scales: indeed, the diameter of a single fibre is roughly 8 μm, while the

space period of the textile arrangement may span several millimetres. Fortunately, all these scales are accessible to X-ray CMT, using classical X-ray sources for the largest ones and Synchrotron Radiation X-ray CMT (XRCT) for the smallest. However, in this last case, one has not a direct access to the density distribution in the material. Indeed, the difference between the absorption coefficients of the carbon fibres, the carbon matrix, the embedding matrix that has sometimes to be used in sample preparation, and air is small and the contrast is faint. Nonetheless, the highly coherent character of the quasi-parallel, monochromatic X-ray beam from synchrotron sources allows for characterizations based on the refractive index contrasts, which are approximately 1000 times larger than the absorption contrasts. [3] Two approaches are then possible: first, the complete refraction index reconstruction, called holotomography, and second, the phase-contrast edge-detection mode, associated to image processing for the segmentation of the constitutive phases. These extra difficulties partly explain why there has been a large time gap between the first successful characterizations of the structure of SiC fibre cloth lay-up preforms at bundle scale (pixel size of 15.6 mm) [4,5] and the same kind of work on C/C composites.

Details on the experimental procedure have been given in refs [6,7]. The samples were raw (CC0 : 73% porosity) and partly infiltrated (CC1 : 50% porosity, CC2 : 23% porosity) C fibre preforms made of stacked satin weaves held together by stitching; they have been scanned with a 0.7 µm voxel edge size resolution, using the setup of the ESRF ID 19 beamline. Lower resolution scans (7.46 µm/voxel) were also made on the same samples, in order to connect with a maximal confidence the fibre-scale and larger scales, like the Representative Elementary Volume (REV) scale. **Figure 1** displays a lower resolution image of the whole sample, the upper part of which has been scanned with higher resolution.

Holotomography results: The first step of holotomographic acquisition[8] is to perform various (3 or 4) classical tomographic acquisitions, with distinct values of the detector-to-sample distance. Then, it is possible to combine together the various projections obtained at the same angle in order to produce a "phase projection" for each angle. Finally, all phase projections are used in a classical reconstruction algorithm, resulting in a 3D map of the imaginary absorption coefficient (or refraction index decrement) δ. Applied to C fibre preforms partially infiltrated with pyrocarbon and embedded in a polycarbonate resin,[6] this yields results as illustrated in **Figure 2**: since δ is closely related to the local material density, it is possible to infer from the δ map a distribution of density, with quantitative values, accurate within 1% error. So, for example, carbon fibres (ρ ~1.7 $g.cm^{-3}$) and pyrocarbon (ρ ~2.0 $g.cm^{-3}$) can be accurately distinguished from each other. Direct segmentation is then feasible, turning easier all posterior image processing and quantification. However, a problem arises in the case of fibres lying perpendicularly to the sample rotation axis: their very high aspect ratio, combined to the strong sensitivity of the detection method, produces blurring artefacts. Indeed, there is a large difference between the phase lag obtained when projecting in parallel and perpendicular directions with respect to these fibres; using only 3 or 4 projections for the phase projection image construction is not enough in this case. So, even if useful local information is available, it is not possible to obtain a full representation of the material.

Phase-contrast edge-detection tomography: The alternative approach is to apply image processing to the tomographic reconstruction obtained with only one set of projections, with a sample-to-detector distance chosen such as Fresnel fringes are clearly visible.[9,10] This provides a strong edge-enhancement effect at any material discontinuity, which has principally been used in a qualitative way. However, there are possibilities of extracting a full representation of the material phases through image processing techniques. In the case of C/C composites, a first algorithm has been developed for the separation of void (or resin) and solid

phases, which display the strongest edge-enhancement effect.[11] It consists in a region-growing algorithm, preceded by a hysteresis step which ensures the continuity of the edge-enhancement pattern. The result of this procedure, applied to a raw fibre preform, is illustrated in **Figure 3**.

Later on, more elaborate techniques have been applied, in the aim of providing a full segmentation of fibres, matrix and void phases. For instance, Martín-Herrero and Germain [12] have designed and successfully tested an algorithm based on a differential profiling method to detect areas between intensity edges on every 2D cross section parallel to the reference system, which are then refined by correlating the outputs in 3D, followed by a "heavy-ball" fibre individuation procedure. Another method [13] uses directly the image gradient (and principally the edge-enhancement patterns) for the estimation of the localization of fibre axes; once the axes have been isolated, a gradient-sensitive region-growing procedure may be applied for the segmentation of the fibres first and then of the matrix. The result of this algorithm is presented in **Figure 4**.

Morphological characterization: Once a proper segmentation of the solid and void phases is available, the first characterisation that can be carried out concerns the geometrical properties of the medium.[7] Pore volume measurements performed on the high-resolution scans have proved to be consistent with experimental determinations; moreover, the convergence towards an REV size has been obtained for volumes larger than 0.03 mm^3 (*i.e.* edge size superior to ~ 0.3 mm). Internal surface area has been determined by a Simplified Marching Cube discretization.[14,15] The total surface area S_V has been found consistent with the experimental values, provided the sub-micrometric roughness contribution (not accessible to this μCT experiment) is removed. Also, the pore size distribution has been evaluated, by application of the traditional formula for elongated pores: $r = 2\varepsilon/S_V$ to each sub-sample. The obtained distribution has been compared to experimental data from Hg intrusion curves, with an excellent agreement, except for large pores,[7,16] as shown in **Figure 5**. Indeed, the reason is

that in the tomography-based estimation, the pore size is limited by the sub-sample size (here, 70 μm). Any larger pore is thus split into pores with dimensions not larger than twice this size.

Characterization of the samples obtained at lesser resolution features two tasks, suited for the modelling targets: the first one is the build-up of a correspondence table between local greyscale values and pore volume fraction, which is principally a matter of data fitting, and the second one is the detection of the local orientation of the fibres. The latter operation has been performed by splitting the blocks into very small sub-volumes, thresholding them arbitrarily to 50% void space, utilizing a random-walk algorithm sensitive to the local anisotropy, and extracting the eigenvectors and eigenvalues of the pseudo-diffusion tensor resulting from the random-walk displacement covariance matrix. The largest eigenvalue indicates the direction of preferred diffusion, which is assimilated to the local fibre orientation (**Figure 6**).

Physico-chemical modelling for CVI based on CMT images

Context: Chemical Vapour Infiltration: Carbon-carbon composites are produced, among other processes, by chemical vapour infiltration (CVI): a heated fibrous preform is infiltrated by the chemical cracking of a vapour precursor of the matrix material inside the pore space of the preform.[17] The quality of materials prepared by CVI relies on processing conditions (such as vapour precursor concentration, temperature and pressure), as well as on intrinsic properties of the preform. Experimental determination of the conditions which lead to an optimal infiltration is time-consuming and expensive. That is the reason why a global modelling of CVI is of great interest to optimize the final density and homogeneity of the composites.[18-23] This modelling requires a good knowledge of geometrical characteristics and transport properties of the preform at various stages of infiltration,[24] namely: the effective gas

diffusivity, either in continuum or in rarefied regime, the gas permeability to viscous flow, and the heat conductivity, in the case of thermal-gradient modifications of CVI.[25]

Gas transport: Effective transport coefficients are calculated in high-resolution images with a random walk algorithm, making use of our surface triangulation scheme[14]. Indeed, there are three diffusion regimes depending on the Knudsen number Kn, which is the ratio between the mean free path of the molecules and the pore diameter : the ordinary regime (Kn << 1), the transition regime (Kn ~ 1), the Knudsen or rarefied regime (Kn >> 1), all three of importance in CVI. The random walk performed by the molecules introduced in the void space is directly linked to the Knudsen number and it allows determining the effective diffusivity tensor $\underline{\underline{D}}$ at any value of Kn. The tortuosity tensor components η_{ij} are then calculated using the equation $\eta_{ij} = \varepsilon D_{ref}./D_{ij}$ where ε is the porosity and D_{ref} the gas diffusivity in void space. **Figure 7** is an example of the results produced by this method for Knudsen transport in transverse direction in numerous sub-samples with 100x100x100 cubic voxels size.[26] The laws that have been fitted to the values computed from the CMT sub-samples have been compared to ideal media made of Boolean sets of straight cylinders:[27] parallel to each other (1D, *i.e.* disorder perpendicular to 1 direction), grouped into mats (2D), or isotropic (3D), with or without overlap between cylinders. Although most of the fibres are rather locally oriented in a parallel fashion, it appears that the 1D models are not the most suited to describe them. Indeed, the discrepancies with the 1D non-overlapping, random cylinder ideal media arises principally from the non-strict alignment between contiguous fibres, a fact which lowers considerably the percolation threshold. So, the actual material laws are intermediate between 1D and 3D.[16] Estimates of the gas transport properties at a larger scale have been performed using a second change-of-scale strategy based on the correlation between greyscale levels and pore space, plus the computation of the local fibre orientation as mentioned earlier. **Figure 8** shows a reasonable agreement with experimental determinations performed in our laboratory.[26]

Heat conduction: In the case of heat conduction, it has been possible to provide a direct comparison with experimental data.[26,28] The microscopic laws have been produced through the study of ideal structures made of an isotropic fibre surrounded by an anisotropic pyrocarbon deposit (with cylindrical symmetry, the radial direction being less conductive), in a periodic unit cell. Values for the individual components have been selected from experimental measurements at LCTS[29] and CEA,[30] and inserted into an effective property computation code working on periodic unit cells. By varying the pyrocarbon volume fraction, taken as (ε_0 - ε), a microscopic-scale law has been produced. Then, the second change of scale performed on low-resolution images with local orientation detection gave predictions in good agreement with direct experimental thermal measurements on the composites,[31] as shown in **Figure 9**.

Infiltration: Finally, an adaptation of the Monte-Carlo Random-Walk algorithm has been designed for the fibre-scale modelling of chemical vapour infiltration.[32] It allows an easy handling of sticking events for the walkers, the sticking coefficient being computed from the diffusion/reaction ratio ; in case of surface growth, the surface triangulation update is fast and efficient thanks to the Simplified Marching Cube algorithm. A closed porosity detecting routine is used to avoid unrealistic pore infiltration. **Figure 10** is an example of infiltration movie obtained on a 100x100x100 cubic voxels image. Moderate values of the mean free path and sticking probabilities have been chosen. The total infiltration has been run in 6 hours 30 on a Pentium4 CPU with 3.2 GHz clock rate. Such a kind of program is able to deliver a precise evolution of the internal surface area and transport properties (diffusivities, etc …) as a function of infiltration progress, which is a valuable tool for large-scale infiltration modelling.[33,34]

Ablation study

Another application domain in which X-ray CMT has proved useful is the study of ablation of C/C composites. This phenomenon is well known to occur when the material is exposed to extreme conditions of heat and chemical aggression, e.g. oxidants. It participates to thermal protection because it is globally endothermic. [35] C/C composites are used as ablative thermal protection systems for atmospheric re-entry and as rocket nozzles because they offer the best performance/weight ratio at the very elevated temperatures to which they are exposed.[1]

Ablation of C/C composites leads to a typical surface roughness which induces enhancement of heat and mass transfer between the protection wall and the surrounding environment via two major phenomena: (i) it increases the chemically active surface of the wall; (ii) it contributes to the laminar-to-turbulent transition in the dynamic boundary layer. The NASA PANT program results show that the heat flux may be multiplied by a factor up to three in turbulent regime.[36] The obvious consequence is a considerable enhancement of global ablation velocity. So, it is of utmost importance to understand what mechanisms lead to the acquisition of a surface roughness and how they work. In this context, a characterization and modelling study has been developed.[37-40] The first step was a qualitative study of the surface morphology, principally based on optical and SEM micrographs, which helped settling the physical bases for the phenomena. Principally, the morphologies are guided by differences of chemical reactivity between constituents and by the competition between heterogeneous transfer (i. e. chemical reaction) and bulk transfer. Analytical [41] and numerical [42,43] simulations of a simple diffusion/reaction model with surface recession have been performed on composites containing fibre bundles perpendicular to the average surface, and the denuded fibre tip height and angle are shown to be in direct relationship with the fibre/weak phase reactivity ratio and to the diffusion/reaction ratio.

Accordingly, a measurement of these parameters on actual surfaces provides an identification of these quantities. Here, high-resolution X-ray CMT is a very interesting tool since it allows easily such measurements. The fact that the images of C/C composites are principally phase contrast images even makes the measurement easier. **Figure 11** displays tomographs of the same material ablated in two ways: the left image is obtained in a simple oxidation test at 625°C,[42] while the right image results from ablation in a plasma jet facility. We can easily see that the Sherwood number, which measures the reaction/diffusion rate ratio, is neatly higher in the second case. This could be expected from the more severe nature of the test in this case.

Conclusion and outlook

This paper has summarized some efforts made in the characterization of C/C composites as a tool for modelling their lifecycle, featuring preparation by chemical vapour infiltration and ablation. High-resolution X-ray tomographic imaging has proved extremely valuable, even though the phase contrast mode was most frequently encountered. The studies have involved image processing and pattern recognition, morphological analysis, and direct numerical simulation of reaction/diffusion systems with moving boundaries. Results show that the assessment of geometrical and transport properties throughout the material evolution is possible on the basis of phase-contrast CMT images; the incorporation of the structure-property relationships in large-scale models of processes and/or degradation tests is indeed of large value and is still currently undergoing.

Further directions are (among others) the development of more adapted holotomographic conditions, like the imaging of samples prepared off-axis with respect to the main fibre directions, and the extension of the computational procedures to larger datasets.

Received: ((will be filled in by the editorial staff))
Revised: ((will be filled in by the editorial staff))
Published online: ((will be filled in by the editorial staff))

References

[1] G. Savage, *Carbon/Carbon composites*, Chapman & Hall, London, **1993**.

[2] H.C. Mantz, D.A. Bowers, F.R. Williams, M.A. Witten, in *Proceedings of IEEE 13th Symposium on Fusion Engineering,* Vol. 2, (Eds. M. S. Lubell, M. B. Nestor, S. F. Vaughan), IEEE, New York, USA IEEE-89CH2820-9, **1990**, 947.

[3] P. Cloetens, W. Ludwig, J. P. Guigay, J. Baruchel, M. Schlenker, D. Van Dyck, in *X-ray tomography in material science* (Eds : J. Baruchel, J.-Y. Buffière, E. Maire, P. Merle, G. Peix,), Hermès, Paris, **2000**, 30.

[4] J. H. Kinney, T. M. Breunig, T. L. Starr, D. Haupt, M. C. Nichols, S. R. Stock, M. D. Butts, R. A. Saroyan, *Science* **1993,** *260*, 789.

[5] S-B. Lee, S. R. Stock, M. D. Butts, T. L. Starr, T. M. Breunig, J. H. Kinney, *J. Mater. Res.* **1998**, *13*, 1209.

[6] O. Coindreau, P. Cloetens, G. L. Vignoles, *Nucl. Instr. and Meth. in Phys. Res. B* **2003**, *200*, 295.

[7] O. Coindreau, G. L. Vignoles, *J. Mater. Res*. **2005**, *20*, 2328.

[8] P. Cloetens, W. Ludwig, J. Baruchel, D. Van Dyck, J. Van Landuyt, J. P. Guigay, M. Schlenker, *Appl. Phys. Lett.* **1999**, *75*, 2912.

[9] M. Ando, S. Hosoya, in *Proc. 6th Intern. Conf. On X-ray Optics and Microanalysis* (Eds. G. Shinoda, K. Kohra, T. Ichinokawa), Univ. of Tokyo Press, Tokyo, **1972**, 63.

[10] P. Cloetens, M. Pateyron-Salomé, J.-Y. Buffière, G. Peix, J. Baruchel, F. Peyrin, M. Schlenker, *J. Appl. Phys.* **1997,** *81*, 5878.

[11] G. L. Vignoles, *Carbon* **2001**, *39*, 167.

[12] J. Martín-Herrero, C. Germain, *Carbon* **2007,** *45*, 1242.

[13] C. Mulat, M. Donias, P. Baylou, G. L. Vignoles, C. Germain, *J. Electronic Imaging* **2008**, *17*, 0311081.

[14] G. L. Vignoles, *J. Phys. IV France* **1995**, *C5*, 159.

[15] M. Donias, G. L. Vignoles, C. Mulat, C. Germain, submitted to *Computational Materials Science,* **2010**.

[16] O. Coindreau, G. L. Vignoles, J.-M. Goyhénèche, in *Advances in Ceramic-Matrix Composites XI* (Eds: N. P. Bansal, J. P. Singh and W. M. Kriven), *Ceram. Trans.* Vol. 175, Wiley, New York, **2005**, 77.

[17] R. Naslain, F. Langlais*, High Temperature Science*, **1990**, *27*, 221.

[18] T. L. Starr, A. W. Smith, *Mat. Res. Soc. Symp. Proc.* **1992,** *250*, 207.

[19] P. McAllister, E. E.Wolf, *AIChE J*., **1993,** *39*, 1196.

[20] G. L. Vignoles, C. Descamps, N. Reuge, *J. Phys. IV France* **2000,** *10*, Pr2-9.

[21] N. Reuge, G. L. Vignoles, *J. Mater. Proc. Technol* **2005,** *166*, 15.

[22] D. Leutard, G. L. Vignoles, F. Lamouroux, B. Bernard, *J. Mater. Synth. and Proc*. **2002**, *9*, 259.

[23] I. Golecki, *Mater. Sci. Eng.* **1997**, *R20*, 37.

[24] J. Y. Ofori, S. V. Sotirchos, *J. Electrochem. Soc.* **1996,** *143*, 1962.

[25] G.L. Vignoles, J.-M. Goyhénèche, P. Sébastian, J.-R. Puiggali, J.-F. Lines, J. Lachaud, P. Delhaès, M. Trinquecoste, *Chem. Eng. Sci.* **2006**, *61*, 5336.

[26] G. L. Vignoles, O. Coindreau, A. Ahmadi, D. Bernard, *J. Mater. Res*. **2007**, *22*, 1537.

[27] M. M. Tomadakis, S. V. Sotirchos, *Mat. Res. Soc. Symp. Proc.* **1992**, *250*, 221.

[28] O. Coindreau, G. L .Vignoles, in *Advanced Materials Forum II* (Eds.: R. Martins, E. Fortunato, I. Ferreira and C. Dias) *Mater. Sci. Forum* Vol. 455-456**,** Trans. Tech. Publications*,* Zurich **2004**, 751.

[29] C. Sauder, PhD dissertation, Université Bordeaux 1 (2001).

[30] J. Jumel, F. Lepoutre, J-P. Roger, G. Neuer, M. Cataldi, F. Enguehardt, *Rev. Sci. Instrum.* **2003,** *74*, 537.

[31] D. Demange, J. C. Laizet, Technical Report RT 1/03519 DMSC, ONERA, Châtillon, France (2000).

[32] C. Mulat, PhD Thesis, University Bordeaux 1, 2008.

[33] G. L. Vignoles, in *Advanced Fibrous Inorganic Composites V* (Ed: P. Vicenzini) *Adv. Sci. Technol.* Vol. 50, Trans Tech Publications, Zürich **2006**, 97.

[34] G. L. Vignoles, C. Germain, O. Coindreau, C. Mulat, W. Ros, in *Proc. ICVD XVII & EuroCVD 17*, (Eds. : M. T. Swihart, D. Barreca, R. A. Adomaitis and K. Wörkhoff), *ECS Transactions* Vol. 25(8), The Electrochemical Society, Pennington, NJ **2009**, 1275.

[35] J. Couzi, J. de Winne, B. Leroy, in *Proc. 3rd Eur. symp. on Aerothermodynamics for space vehicles* (Ed.: K. Fletcher) ESA Publications, Noordwijk, The Netherlands **1998**, 493.

[36] M. D. Jackson MD. Report SAMSO-TR7486 of Passive Nosetip Technology (PANT) Program No. 15, **1974**.

[37] Y. Aspa, M. Quintard, F. Plazanet, C. Descamps, G. L. Vignoles, in *Mechanical Properties and Performance of Engineering Ceramics and Composites*, (Eds.: E. Lara-Curzio, D. Zhu, W. M. Kriven), *Ceram. Eng. and Sci. Proc.* Vol. 26(2), Wiley, New York **2005**, 99.

[38] J. Lachaud, G. L. Vignoles, J.-M. Goyheneche, J.-F. Epherre, in *Thermochemistry and Metrology of Interfaces*, (Ed.: L. P. Cook), *Ceram. Trans.* Vol. 191, The American Ceramic Society, Westerville, OH **2005,** 149.

[39] G. L. Vignoles, J. Lachaud And Y. Aspa, in *Proc. 5th European Workshop on Thermal Protection Systems and Hot Structures*, (Ed.: K. Fletcher), *ESA Conf. Procs.* SP-631, ESA Publications, Noordwijk, The Netherlands **2006** (CDROM)

[38] G. L. Vignoles, J. Lachaud, Y. Aspa, J.-M. Goyhénèche, *Compos. Sci. and Technol.* **2009**, *69*, 1470.

[39] J. Lachaud, Y. Aspa, G. L. Vignoles, *Int. J. Heat and Mass Transfer* **2008**, *51*, 2614.

[40] Y. Aspa, J. Lachaud, G. L. Vignoles, M. Quintard, in *Proc. 9th joint AIAA/ASME Thermophysics and Heat Transfer Conference*, (Eds.: J. E. Haas, M. P. Wernet, E. Marotta, Y. Joshi) *AIAA Papers* **2006** ref. 2006-2911, 52

[41] J. Lachaud, G. L. Vignoles, *Comput. Mater. Sci.* **2008**, *44*, 1034.

[42] J. Lachaud, N. Bertrand, G. L. Vignoles, G. Bourget, F. Rebillat, P. Weisbecker, *Carbon* **2007**,*45*, 2768.

Fig. 1. C/C sample for CT acquisition at 2 distinct resolutions. Sample outer diameter is 6 mm. Low-resolution scan of the sample: 1 voxel = 7.46 µm.

Fig. 2. Visualizations of C/C sample CC2, as scanned by holotomography. Resolution is 0.7 µm per voxel. Fibres, matrix and void space are directly segmentable in the perpendicular bundles. Parallel bundles are blurred. a) 3D rendering ; b) 2D slice (detail).

Fig. 3. Segmentation of C fibres in sample CC0 (raw preform) from an edge-detection tomograph. Resolution is 0.7 µm/voxel. a) Slice of the original data set. b) 3D rendering.

Fig. 4. Segmentation of fibres and matrix in C/C sample CC2 from an edge-detection mode tomography, after fibre shape recognition. Resolution is 0.7 µm/voxel. a) Detail of a slice of the original data (after median filtering), b) 3D rendering of the segmented data.

Fig. 5. Comparison of Hg intrusion data: modelled on C/C sample CC1 (50% porosity) and experimental on another one from the same infiltration run with ~50% pore volume fraction.

Fig. 6: Visual inspection of the efficiency of the local anisotropy detector: the direction of highest conductivity is determined on 7×7×7-voxel size zones and are plotted by preferential orientation.

Fig. 7. Tortuosity–porosity correlation plots for Knudsen transport in transverse direction. Comparison of CMT data with correlations for ideal fibrous media.

Fig. 8. Comparison of computed and experimental values of Knudsen diffusivities. Directions are given relatively to the ply stacking direction.

Fig. 9. Comparison of computed and experimental values of thermal conductivities. Directions are given relatively to the ply stacking direction.

Fig. 10. An example of infiltration simulation in a 100x100x100 block. Mean free path is 1 voxel (0.7 µm); sticking probability is 0.166. The graph is the evolution of the scaled Thiele modulus $\Phi/\Phi_0 = \sqrt{\frac{S_v}{D}\frac{D_0}{S_{v0}}}$ *as the pore volume decreases. (*S_V *is the internal surface area,* D *is the diffusivity, and 0 refers to initial values)*

Fig. 11. Identification from X-ray CMT slices of the reaction/diffusion ratio on samples of a C/C composite ablated in different conditions : left, oxidation in mild conditions, top, plasma jet ablation. The right side shows the numerical and analytical results of a simple model giving the relation between the shape of the fiber tip and the reaction-to-diffusion ratio (Sherwood number) [41].

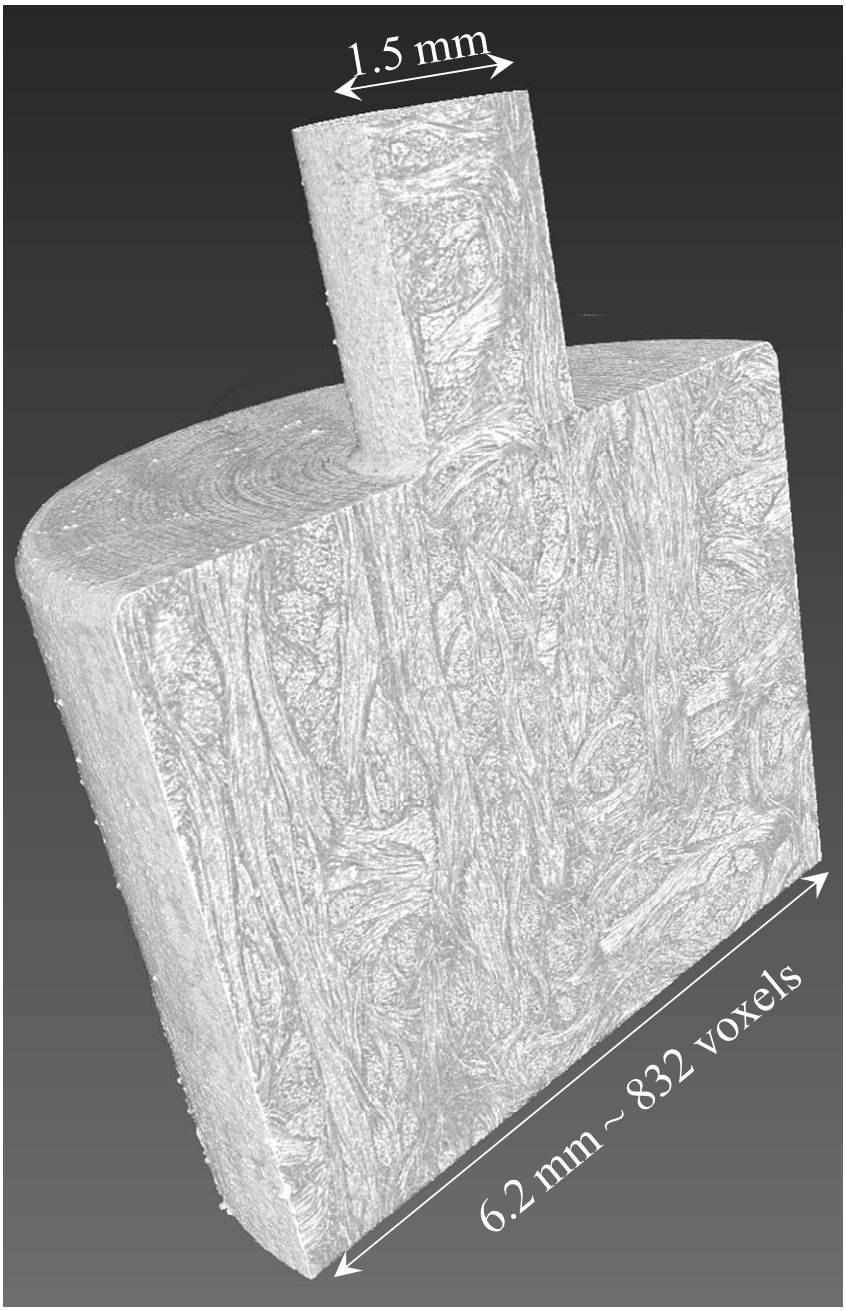

Fig. 1. C/C sample for CT acquisition at 2 distinct resolutions. Sample outer diameter is 6 mm. Low-resolution scan of the sample: 1 voxel = 7.46 µm.

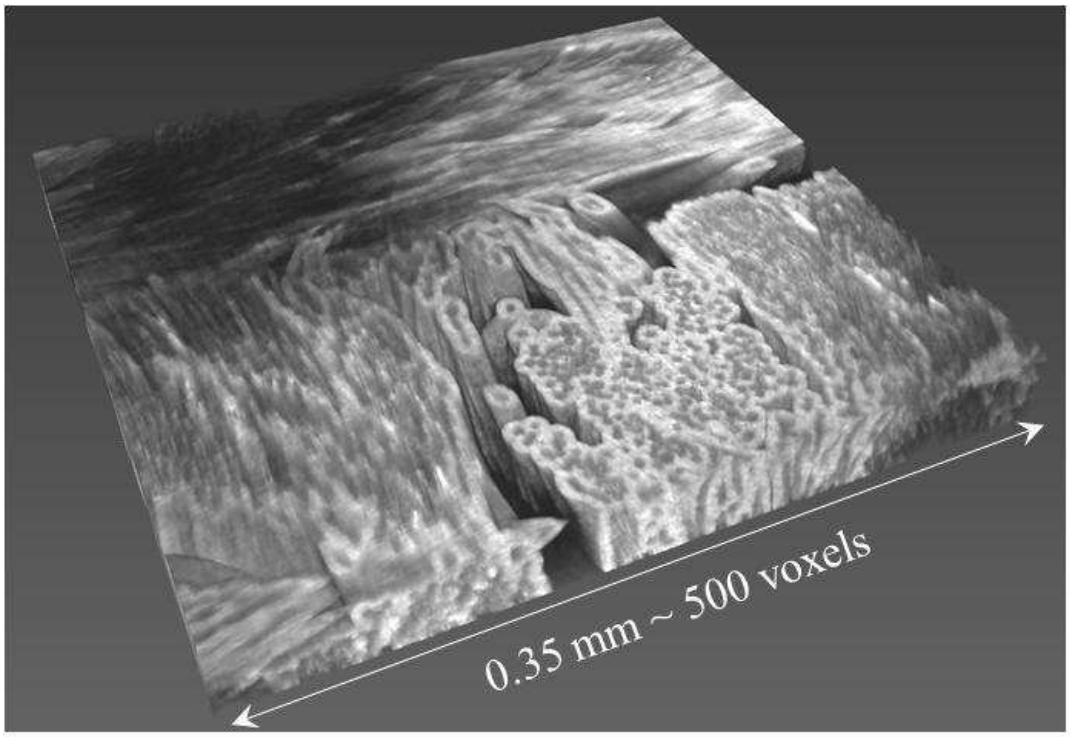

a)

b)

Fig. 2. Visualizations of C/C sample CC2, as scanned by holotomography. Resolution is 0.7 µm per voxel. Fibres, matrix and void space are directly segmentable in the perpendicular bundles. Parallel bundles are blurred. a) 3D rendering ; b) 2D slice (detail).

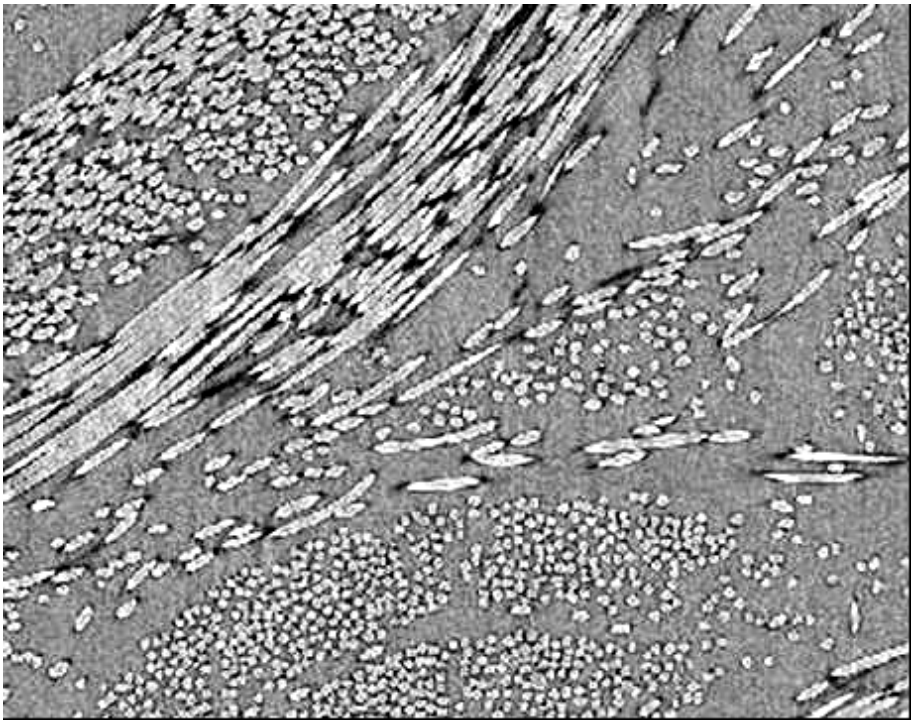

a)

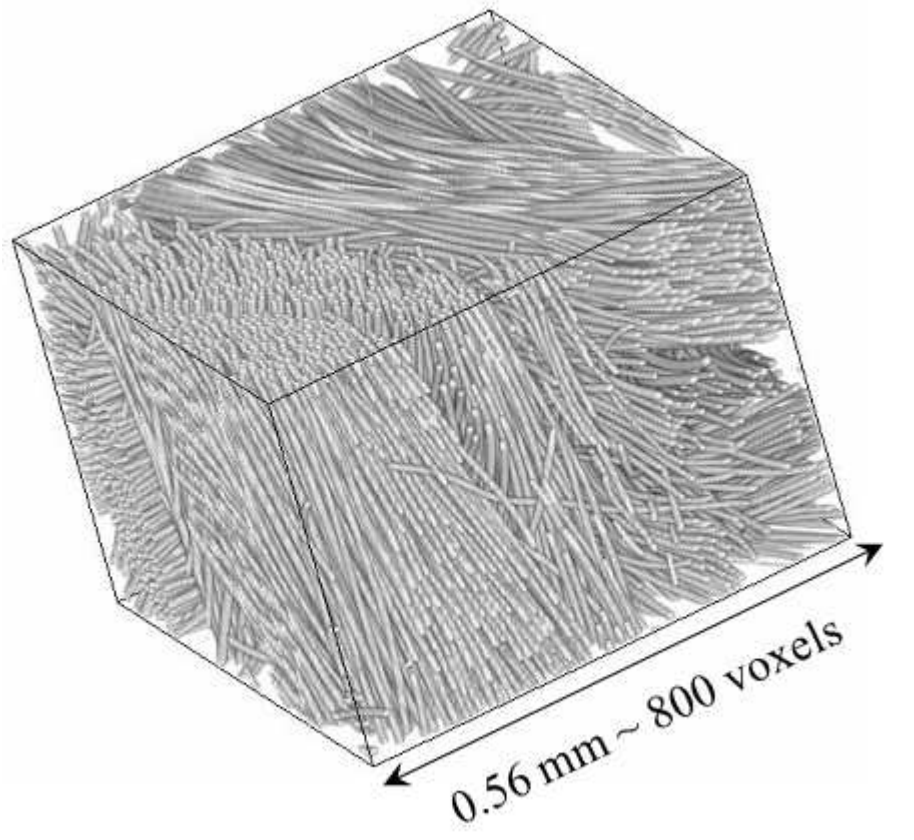

b)

Fig. 3. Segmentation of C fibres in sample CC0 (raw preform) from an edge-detection tomograph. Resolution is 0.7 µm/voxel. a) Slice of the original data set. b) 3D rendering.

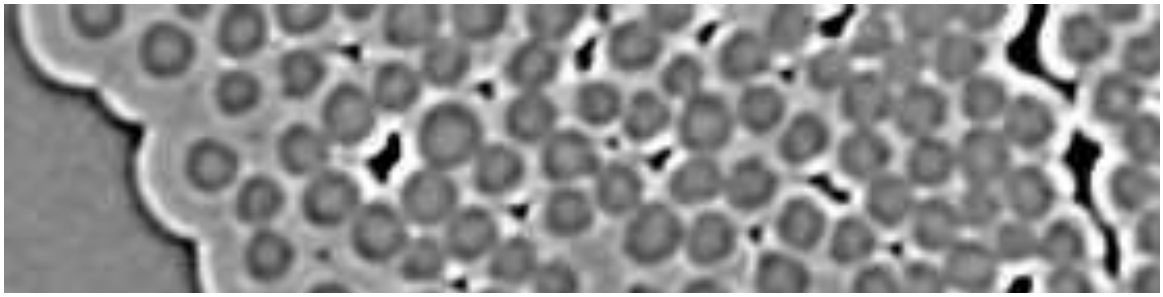

a)

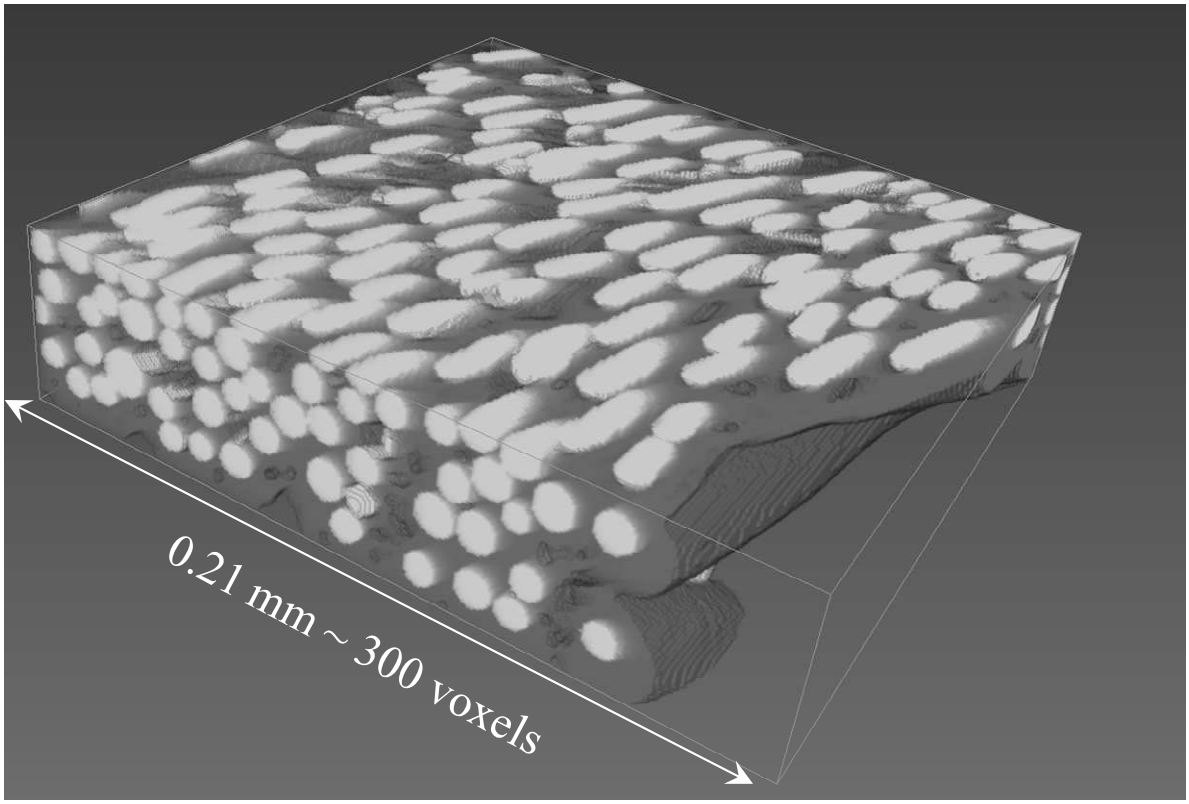

b)

Fig. 4. Segmentation of fibres and matrix in C/C sample CC2 from an edge-detection mode tomography, after fibre shape recognition. Resolution is 0.7 µm/voxel. a) Detail of a slice of the original data (after median filtering), b) 3D rendering of the segmented data.

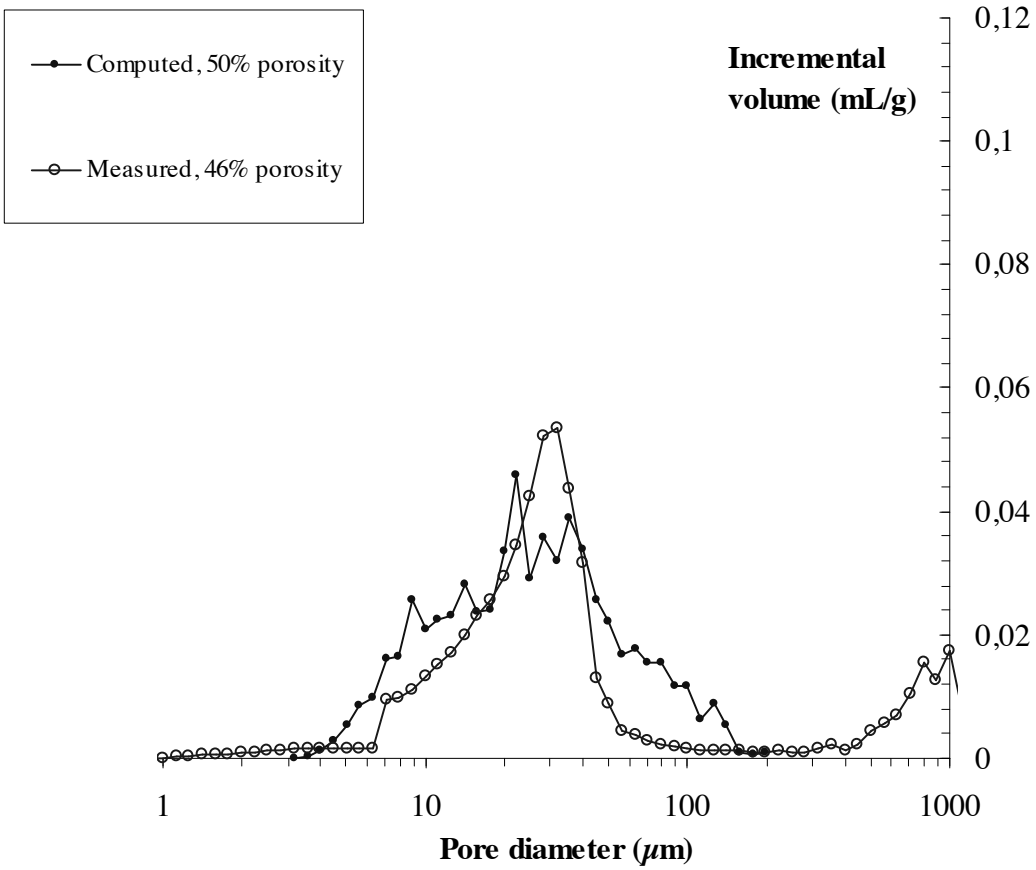

Fig. 5. Comparison of Hg intrusion data: modelled on C/C sample CC1 (50% porosity) and experimental on another one from the same infiltration run with ~50% pore volume fraction.

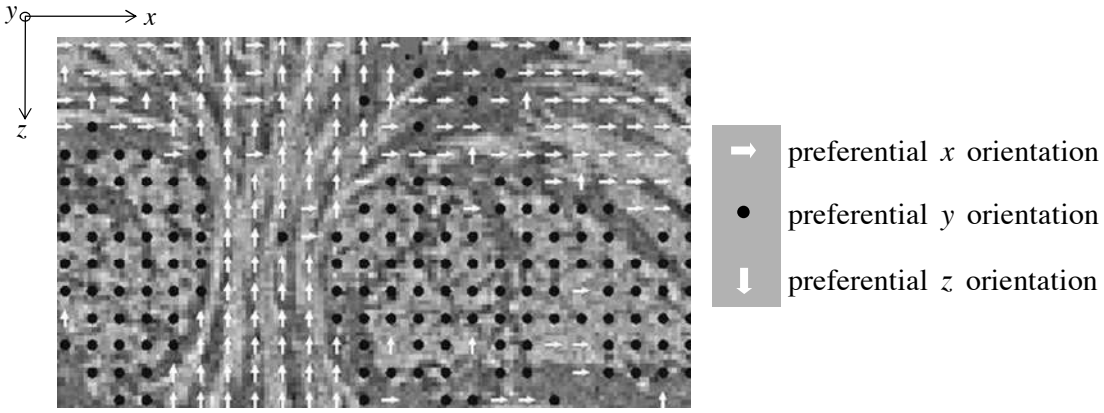

Fig. 6: Visual inspection of the efficiency of the local anisotropy detector: the direction of highest conductivity is determined on 7×7×7-voxel size zones and are plotted by preferential orientation.

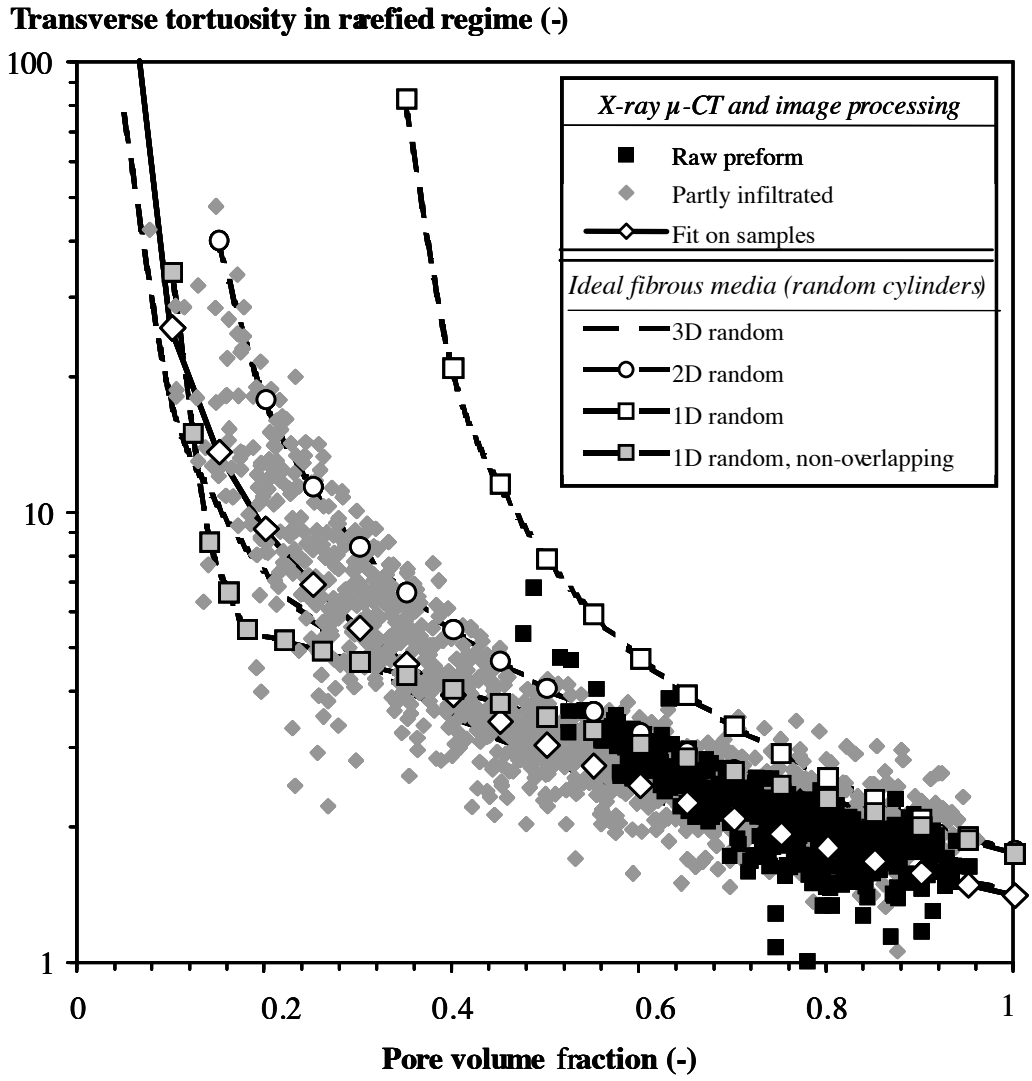

Fig. 7. Tortuosity–porosity correlation plots for Knudsen transport in transverse direction. Comparison of CMT data with correlations for ideal fibrous media.

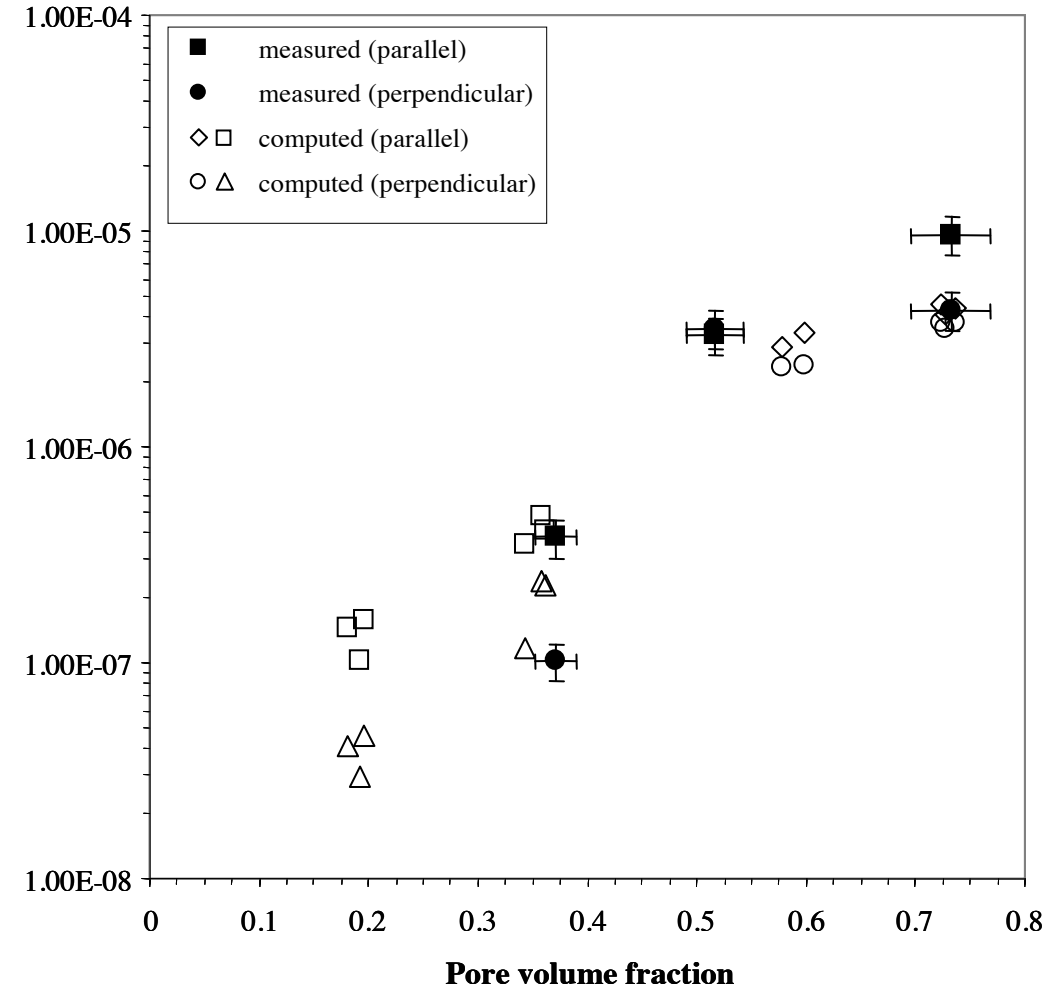

Fig. 8. Comparison of computed and experimental values of Knudsen diffusivities. Directions are given relatively to the ply stacking direction.

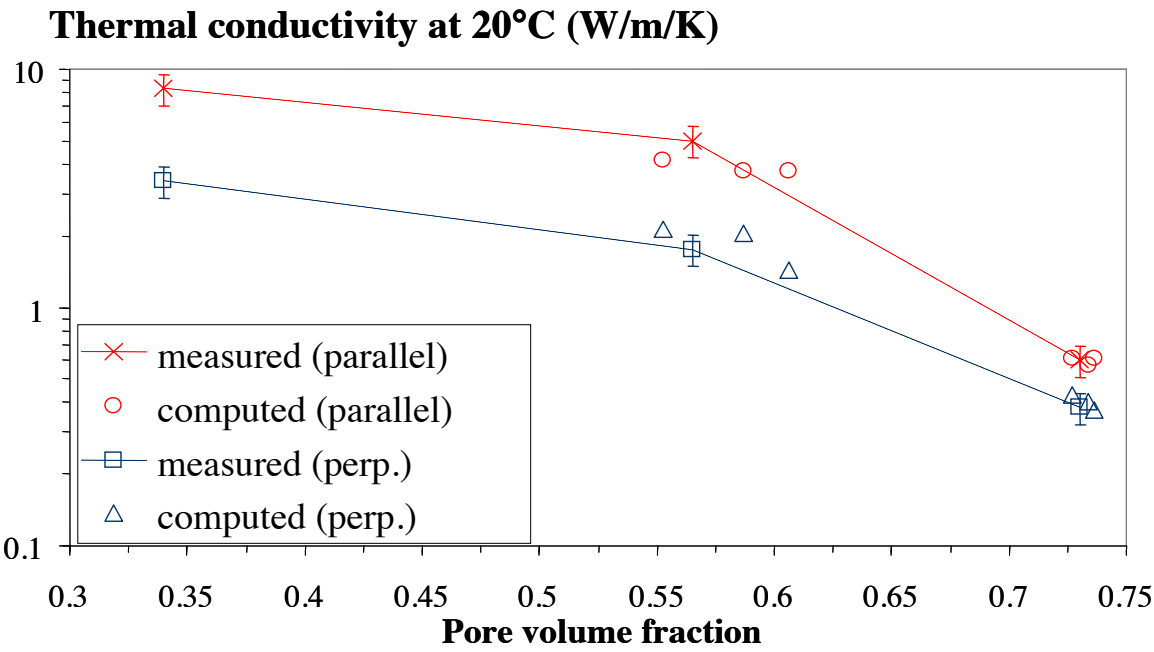

Fig. 9. Comparison of computed and experimental values of thermal conductivities. Directions are given relatively to the ply stacking direction.

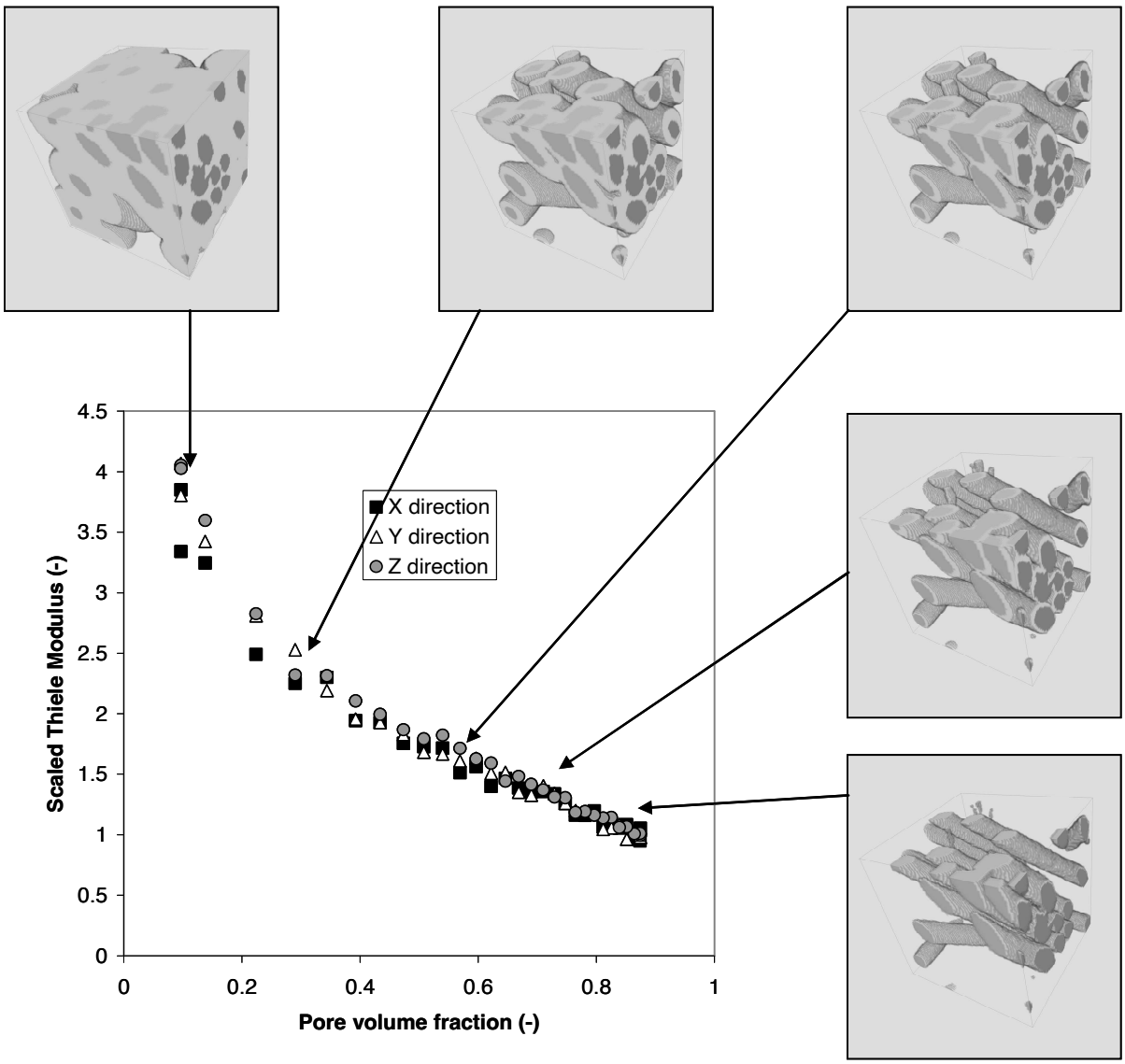

Fig. 10. An example of infiltration simulation in a 100x100x100 block. Mean free path : 1 voxel (0.7 µm) ; sticking probability : 0.166. The graph is the evolution of the scaled Thiele modulus $\Phi / \Phi_0 = \sqrt{\frac{S_v}{D}\frac{D_0}{S_{v0}}}$ *as the pore volume decreases. (S_V is the internal surface area, D is the diffusivity, and 0 refers to initial values)*

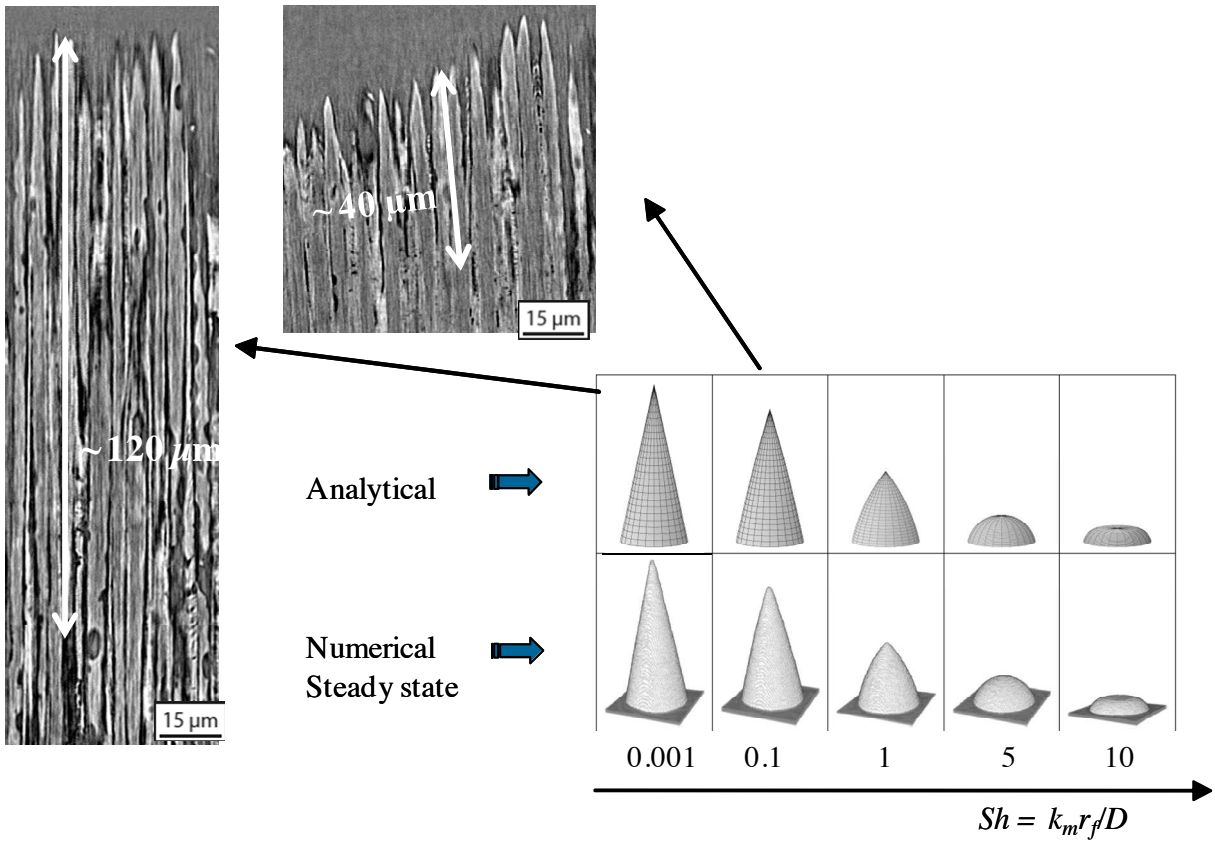

Fig. 11. Identification from X-ray CMT slices of the reaction/diffusion ratio on samples of a C/C composite ablated in different conditions : left, oxidation in mild conditions, top, plasma jet ablation. The right side shows the numerical and analytical results of a simple model giving the relation between the shape of the fiber tip and the reaction-to-diffusion ratio (Sherwood number) [41].

The table of contents entry should approximately one hundred words, written in the present tense, and refer to the chosen figure.

O. Coindreau, C. Mulat, C. Germain, J. Lachaud, and G. L. Vignoles*■<B>…<B>■

Benefits of X-ray CMT for the modelling of C/C composites

This article summarizes and discusses holotomographic and phase-contrast X-ray Tomographic imaging of C/C composites performed at two resolutions, and subsequent computations of geometrical and transport properties, as well as simulations, *e.g.* of the modelling of matrix processing by chemical vapour infiltration.